Research Square

Preprints are preliminary reports that have not undergone peer review.
They should not be considered conclusive, used to inform clinical practice,
or referenced by the media as validated information.

Mechanistic Insights into Plasma-Liquid Interfacial Degradation of Perfluorooctanoic Acid (PFOA) in an Argon RF Plasma Jet

Md Akibur Rahman
Clarkson University
Thomas M. Holsen
Clarkson University
Selma Mededovic Thagard
smededov@clarkson.edu
Clarkson University

Research Article

Keywords: atmospheric pressure plasma jet, degradation, PFOA, plasma-liquid interface, water treatment

Posted Date: April 10th, 2026

DOI: https://doi.org/10.21203/rs.3.rs-9172359/v1

License: This work is licensed under a Creative Commons Attribution 4.0 International License.
Read Full License

Additional Declarations: No competing interests reported.

Mechanistic Insights into Plasma-Liquid Interfacial Degradation of Perfluorooctanoic Acid (PFOA) in an Argon RF Plasma Jet

Md Akibur Rahman[1], Thomas M. Holsen[2], and Selma Mededovic Thagard[1]*

[1]Department of Chemical and Biomolecular Engineering, Clarkson University, Potsdam, New York, 13699, USA

[2]Department of Civil and Environmental Engineering, Clarkson University, Potsdam, New York, 13699, USA

Corresponding author* Email: smededov@clarkson.edu; Tel: +1 315-268-4423

Abstract

Radio frequency (RF) driven atmospheric pressure plasma jets (APPJs) operate in a non-equilibrium regime that enables highly localized energy deposition and reactive species delivery to gas-liquid interfaces. In this study, 10 mg L^{-1} perfluorooctanoic acid (PFOA) was treated in a 13.5 mL recirculating, flow-through reactor contacted by an RF argon APPJ. The parent PFOA was removed to below detection within two hours, while fluoride release continued and reached up to ~80% after three hours. Identified short-chain perfluoroalkyl acids (C_2-C_7) accounted for ~12% of the initial mass. Systematic variation of discharge power, liquid flowrate, radical and electron scavengers, and processing gas composition was used to elucidate the dominant degradation pathways. PFOA removal was unaffected by liquid flowrate but increased with discharge power, indicating that degradation is controlled by interfacial plasma processes rather than bulk hydrodynamic transport. Fluorine mass balance and scavenger experiments demonstrate that the majority of fluoride release (>70%) occurs directly during the initial interfacial dissociation of parent PFOA, driven by plasma-generated species. Hydroxyl radical scavenging had no effect on PFOA degradation but significantly suppressed fluoride formation, indicating a secondary role in oxidizing partially fluorinated intermediates. In contrast, $AgNO_3$, a solvated-electron probe, produced minimal changes in degradation or defluorination trends. Gas substitution experiments (Ar, He, Ar/H_2, Ar/N_2) revealed substantially reduced defluorination in helium, supporting a mechanistic picture in which dominant initiating steps occur near the plasma-liquid interface and depend on gas-phase discharge characteristics, particularly electron density and vacuum ultraviolet (VUV) photon flux generation.

Keywords: atmospheric pressure plasma jet, degradation, PFOA, plasma-liquid interface, water treatment

1. Introduction

Per- and polyfluoroalkyl substances (PFAS) are a group of anthropogenic chemicals that have been widely used in diverse industrial and consumer applications, including non-stick cookware, stain-resistant fabrics, waterproofing treatments, firefighting foams, and many other applications [1]. They exhibit persistent behavior in the environment, leading to their accumulation in water, soil, wildlife, and human blood samples worldwide [2]. Exposure to PFAS has been associated with adverse health effects, including kidney and testicular cancer, thyroid disease, immune system dysfunction, decreased fertility, developmental delays in children, among others [3]. In response to these risks, the United States Environmental Protection Agency (USEPA) finalized the first enforceable national drinking water standards for PFAS in 2024. These regulations establish maximum contaminant levels (MCLs) of 4 ng/L for both perfluorooctanoic acid (PFOA) and perfluorooctane sulfonate (PFOS), and 10 ng/L for perfluorononanoic acid (PFNA), perfluorohexane sulfonate (PFHxS), and the HFPO-DA "GenX" chemicals. In addition, USEPA introduced a hazard-index–based standard for mixtures of PFNA, PFHxS, PFBS, and GenX, reflecting growing recognition that PFAS occur and act as complex chemical mixtures rather than isolated compounds [4]. Ongoing research efforts are focused on developing safer alternatives to PFAS and exploring effective remediation methods for PFAS-contaminated sites and water sources [2].

Conventional water treatment methods for PFAS include activated carbon filtration, ion exchange, and membrane processes. While these non-destructive methods are effective, they have limitations such as poor adsorption capacity, resin regeneration requirements, high energy consumption, and membrane fouling [5]. Moreover, they generate a PFAS residue that must be further disposed of. Non-thermal electrical discharge plasma technology, which is capable of breaking the carbon-fluorine bonds, offers a promising alternative for the treatment of these compounds [6]. Furthermore, electrical plasmas have been recognized as one of the most effective and efficient technologies available today for degrading long-chain PFAS, such as PFOA [7]. However, the elementary steps governing PFOA degradation, particularly the relative roles of interfacial electron-, ion-, and photon-driven processes versus bulk aqueous chemistry, remain largely unknown. Because PFAS are resistant to conventional oxidation, plasma-driven degradation has been attributed to species generated near the plasma-liquid interface, including electrons, ions, metastables, and vacuum-ultraviolet (VUV) photons, rather than to bulk-phase aqueous oxidants [8–12]. Numerous plasma studies have reported the stepwise degradation of the parent compound (e.g., PFOA, a C_8 compound), leading to the generation of C_2-C_7 short-chain perfluoroalkyl acids, fluoride ions and gaseous byproducts [5, 8, 12]. While the

ultimate objective of the treatment is complete PFAS mineralization (i.e., 100% defluorination), no plasma reactor or excitation source has been able to achieve this level of success [5, 13, 14]. Moreover, while a wide range of plasma configurations have been investigated, plasma jets, particularly those directly interfacing with liquids, have received comparatively limited attention for PFAS degradation [15]. In plasma jets contacting liquids, reactive species are delivered to a *nm*-scale interfacial region where electric fields, surface charge accumulation, and surfactant enrichment can strongly localize reactivity [16–19]. In this context, the primary objective of this work was to explore PFOA degradation using a radio frequency (RF) driven atmospheric pressure plasma jet (APPJ). The focus was placed on the identification and quantification of liquid-phase degradation byproducts, closing the fluorine mass balance, and identification of the key species contributing to degradation and defluorination.

2. Materials and Methods

2.1 Chemicals

Perfluorooctanoic acid (PFOA, reagent grade, 95% purity), phenol (molecular biology grade), and silver nitrate ($AgNO_3$, anhydrous, ≥ 99.99% trace metals basis) were purchased from Sigma-Aldrich and used as received. Deionized water of conductivity 1 μS/cm was used for the preparation of all solutions. Helium (99.99% purity), argon (99.99% purity), nitrogen (99.99% purity), and hydrogen (5% H_2 balanced with argon, industrial grade mix) gas cylinders were purchased from Airgas.

2.2 Experimental setup

Fig. 1 shows the overall experimental setup. Plasma was generated using an RF generator (T&C Power Conversion AG – 0113R) with a continuous sinusoidal voltage waveform at a frequency of 13.56 MHz. A matching box (T&C Power Conversion AIT – 600) was connected in series between the high voltage output of the power generator and the APPJ to match the generator to the APPJ. As shown in Fig. 1, a directional coupler between the matching box and the APPJ was connected to an oscilloscope to measure the discharge voltage. The APPJ consisted of a tungsten needle electrode (ø = 1 mm) encased in a quartz tube (2 mm (ID) × 3 mm (OD)) and a grounded ring electrode (3.15 mm (ID) × 4.76 mm (OD) × 5.4 mm (H)) placed around the quartz tube. Throughout the experiments, the ground-to-nozzle and electrode-to-nozzle distances were 2 mm and 1 mm, respectively. For all experiments, the distance between the jet nozzle outlet and the liquid surface was consistently maintained at 2 mm to ensure plasma-liquid touching conditions. The working gas was ultra-high purity grade (≥ 99.99%) argon flowing at 0.8 SLM. In certain experiments argon was replaced with ultra-high purity helium, nitrogen and hydrogen. In the experiments

involving a 0.4% N_2 (or, 1% H_2) balanced with Ar, an additional mass flowmeter was used for the N_2 gas line and a gas manifold that served as a temporary reservoir was used to mix the gases before introducing them to the jet. All experiments were conducted at a discharge power of 60 W. However, it is worth noting that the actual power delivered to the jet might have been substantially lower, potentially by an order of magnitude, owing to excessive reflective power. This observation is supported by the significant heating experienced by the cable connecting the RF generator to the matching box, indicative of power dissipation.

Working PFOA solution was treated in a 3 mL flow-through reactor (type 48 quartz cell) equipped with two side tubes which served as inlets and outlets, as shown in Fig. 1. The flow-through cell had outer dimensions of 45 mm (L) × 12.5 mm (W) × 12.5 mm (H). The side tubes with a dimension of 3 mm (ID) × 5 mm (OD) served as the inlet and outlet of the reactor. A peristaltic pump (Masterflex L/S 77200-60) was incorporated into the setup to introduce mixing. An external sample reservoir system of 13.5 mL was implemented to address the challenges posed by continuous solution level depletion due to evaporation and the requirement for external mixing. The liquid in the reactor was recirculated at 15 mL/min or 145 mL/min, depending on the experiment. Precise measurements of the flowrates were performed using a graduated cylinder and a timer. It is important to note that, unless explicitly indicated otherwise, all results presented in this study correspond to a liquid flowrate of 15 mL/min and a total solution volume of 13.5 mL.

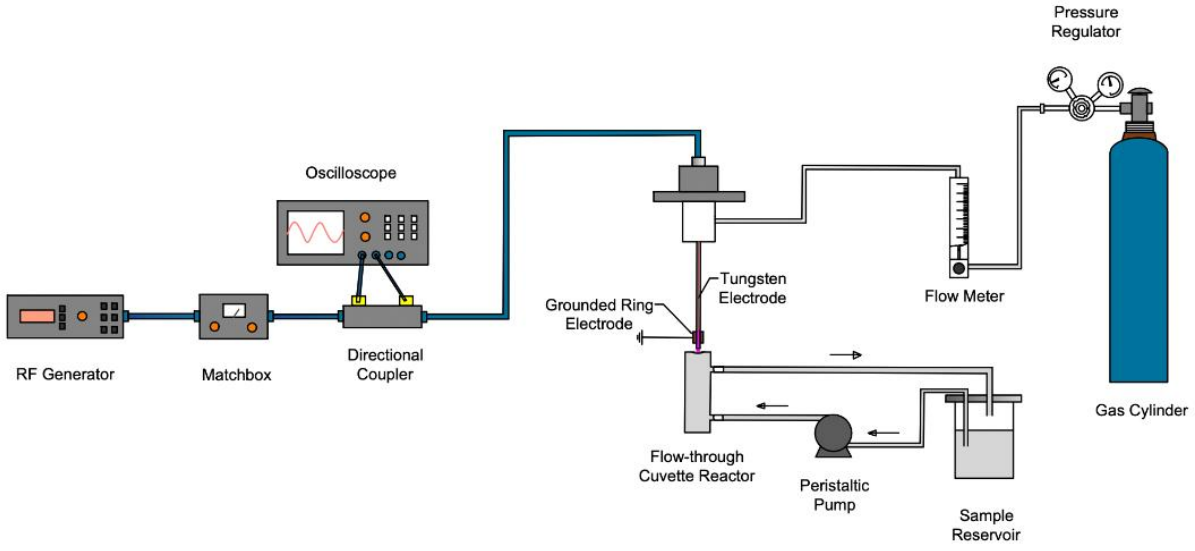


Fig. 1 Schematic of the overall experimental setup featuring an RF plasma generating network, atmospheric pressure plasma jet, and flow-through reactor setup.

2.3 Experimental procedures

Perfluorooctanoic acid solutions with an initial concentration of 10 mg/L (~24 µM) were prepared using deionized water without any adjustments to the solution's electrical conductivity, which remained in the range of ~1 µS/cm. The reactor was filled with a sample volume of 13.5 mL and then carefully positioned on a translation stage (not shown in Fig. 1) underneath the plasma jet. Prior to starting each experiment, the solution was circulated within the flow-through reactor system for 5 minutes. Considering that the volume of the treated liquid required for analyses was 1 mL, a single sample collection was conducted at the conclusion of the treatment. Consequently, multiple distinct experiments were performed, ranging from the initial point (t = 0 min) to reach specific target treatment times, thereby enabling the acquisition of time-resolved degradation profiles at 20-minute intervals. For all the experimental conditions, the PFOA removal followed pseudo first-order kinetics, as described by Equation (1) [20]:

$$-\frac{dC_{PFOA}}{dt} = k_{obs} C_{PFOA} \tag{1}$$

where C_{PFOA} [mol/L] represents the concentration of a PFOA at time t, and k_{obs} [min^{-1}] is the experimentally derived (observed) rate constant. Fluoride formation also followed pseudo first-order kinetics, as described by Equation (2):

$$C_{F^-}(t) = C_{F^-,\infty}(1 - e^{-k_{F^-}t}) \tag{2}$$

where $C_{F^-}(t)$ [mol/L] represents the concentration of fluoride ions at time t, $C_{F^-,\infty}$ [mol/L] is the asymptotic (final) fluoride concentration as $t \rightarrow \infty$, and k_{F^-} [min^{-1}] is the observed rate constant for fluoride release. The extent of defluorination for all PFAS compounds is quantified using Equation (3) [21]:

$$Fluoride_yield(\%) = \frac{C_{F^-}}{C_0 \times N_{C-F}} \tag{3}$$

where C_{F^-} [mol/L] is the measured fluoride concentration, C_0 [mol/L] is the initial concentration of the parent PFAS, and N_{C-F} is the number of C-F bonds in the parent PFAS molecule.

2.4 Analytical methods

Perfluoroalkyl acids (PFAAs) bulk liquid concentrations were determined using an ultra-performance liquid chromatography-mass spectrometry (UPLC-MS-MS) system (Thermo Scientific Vanquish-TSQ ALTIS). The instrument was equipped with a pentafluorophenylpropyl (PFP) Accucore C18 column (2.1 mm × 100 mm, 2.6 µm) and a 20 µL injection loop. The gradient solvent program utilized consisted of 5 mM ammonium acetate and LCMS-grade acetonitrile. All samples underwent a triple dilution with a mixture composed of 75% methanol and 25% water.

Following this, the samples were analyzed by electrospray in negative ion mode. Fluoride (F^-) ion concentrations were measured using an Ion Chromatograph (Dionex Integrion HPIC) equipped with a Fast Hydroxide-Selective Anion-Exchange AS18 column (Dionex Ionpac 4 x 150 mm, RFIC, Analytical, 4 μm). The analysis was carried out under isocratic conditions using potassium hydroxide solution as the eluent at a constant flow rate of 0.75 mL/min. The electrical conductivity and pH of the solution before and after the plasma treatment were measured using a conductivity meter (OAKTON, Cole-Palmer Model 35604-00) and a pH probe (Apera Instruments LLC), respectively. The concentration of hydrogen peroxide generated by the plasma was measured colorimetrically at 409 nm using a UV-Vis spectrophotometer (UV-1900i, Shimadzu) [22].

3. Results

3.1 The effect of liquid flowrate and discharge power on the degradation and defluorination of PFOA

Fig. 2 shows the dependence of the PFOA degradation (a) and fluoride ions concentration (b) on liquid flowrate and discharge power. Control experiments conducted without plasma revealed that the liquid evaporation induced by the impinging gas contributed to ~8% loss of the solution volume after 180 minutes of treatment. To account for this, all solution concentrations were corrected based on the measured final volumes so that the reported concentrations represent the true solute levels during treatment. Results indicate that for a fixed discharge power of either 45 or 60 W, an increase in the liquid flowrate from 15 to 145 mL/min had a minimal effect on the PFOA degradation and fluoride yield (Table 1). By contrast, increasing the discharge power from 45 to 60 W increased the degradation rate constant by ~35% and the fluoride yield by ~15-20%.

Table 1 Experimentally derived rate constants for the four distinct experimental conditions of power and liquid flow which are shown in Fig. 2.

Experimental condition	Observed degradation rate constant, k_{obs} (min^{-1})	Fluoride ion production			Fluoride yield at t = 180 min (%)
		$C_{F^-,\infty}$ (mM)	Initial rate (μM/min)	Observed rate constant for fluoride release (min^{-1})	
45 W @15 mL/min	0.018	0.33	3.2	0.010	66
45 W @145 mL/min	0.019	0.33	3.0	0.009	61
60 W @15 mL/min	0.025	0.37	4.5	0.012	80
60 W @145 mL/min	0.024	0.36	4.7	0.013	81

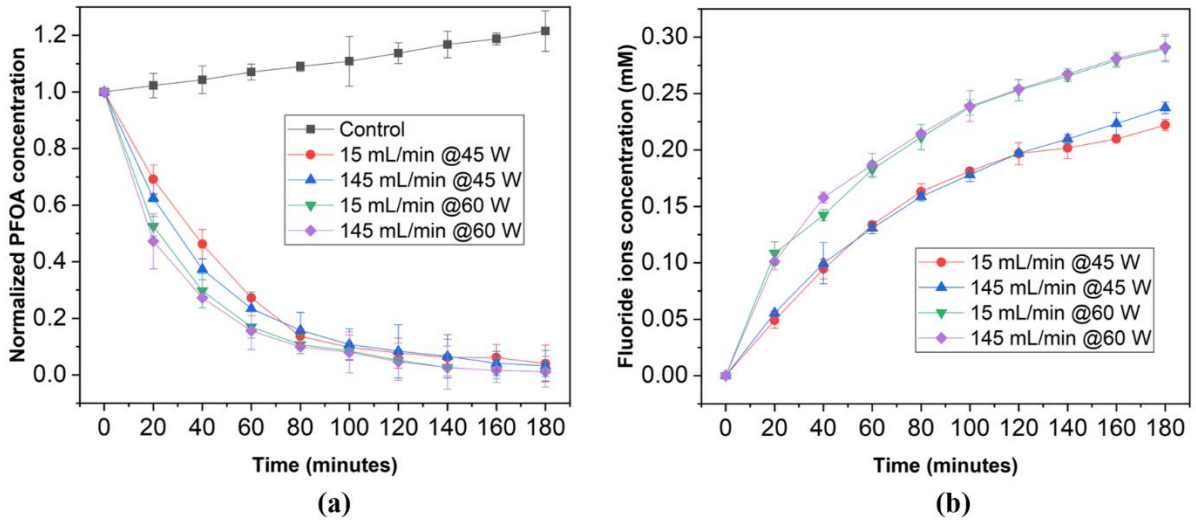


Fig. 2 Time-dependent (a) normalized PFOA concentration and (b) fluoride ions concentration for two different discharge power and liquid flowrates. Control experiment was conducted under continuous gas flow without plasma.

While the specific plasma species responsible for PFOA degradation remain unknown, the observed increase in degradation rate and fluoride yield with increasing discharge power indicates that the interfacial flux of reactive species delivered to the liquid surface increases with power input. This interpretation is consistent with the H_2O_2 measurements shown in Fig. 3, where higher power resulted in significantly greater concentrations of hydrogen peroxide. H_2O_2 serves here as an indicator of overall plasma oxidative activity; however, its formation primarily reflects time-integrated secondary aqueous-phase chemistry rather than the interfacial processes responsible for initiating PFOA degradation [23–25]. Although OH radicals, which are directly involved in H_2O_2 formation, are not believed to play a dominant role in PFOA degradation, their potential involvement in downstream oxidation and defluorination of intermediate products cannot be ruled out and is discussed further in Section 3.2.

The minimal impact of the liquid flowrate on the degradation of PFOA using a plasma jet is consistent with an interfacial, flux-limited reaction regime rather than bulk transport control. Because the plasma-liquid contact area is limited and the delivery of reactive species is governed primarily by plasma-generated fluxes, increasing the liquid flowrate does not significantly increase degradation. Previous modeling efforts have demonstrated that for gas plasmas contacting liquids, contaminant degradation is strongly affected by both the magnitude of the plasma area and the rate of liquid surface renewal rate under the plasma, depending on reactor conditions [26–28]. For large plasma areas spanning several cm^2, degradation exhibits the highest degree of sensitivity to fluid flow under the plasma. For smaller plasma areas, typically ≤ 0.5 cm^2, the removal is unaffected by the variations in liquid flow [26]. Since PFOA

preferentially accumulates at the plasma-liquid interface due to its amphiphilic nature, its degradation is decoupled from conventional diffusional and convective transport limitations and governed primarily by near-surface processes [2, 5–7]. The relatively minor impact of liquid flowrate on PFOA degradation is further supported by H_2O_2 measurements, which indicate that H_2O_2 production is nearly independent of the liquid flowrate (Fig. 3).

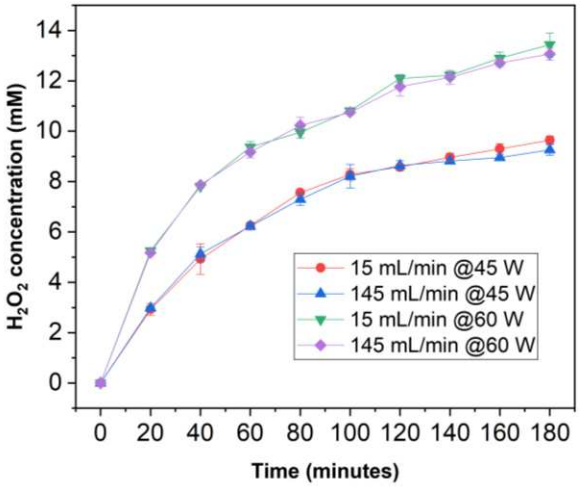


Fig. 3 Time-dependent H_2O_2 concentration profiles measured in deionized water for two different discharge power inputs and liquid flowrates.

In addition to fluoride ions, the degradation of PFOA resulted in a generation of short-chain perfluoroalkyl acids (PFAAs), including perfluoroheptanoic acid (PFHpA, C_7), perfluorohexanoic acid (PFHxA, C_6), perfluoropentanoic acid (PFPeA, C_5), perfluorobutanoic acid (PFBA, C_4), perfluoropropionic acid (PFPA, C_3), and trifluoroacetate (TFA, C_2) (Fig. 4a). The presence of these compounds has been previously reported in earlier plasma studies, and the degradation pathways leading to their formation have been elucidated through the stepwise degradation of PFOA [29–32]. Note that experiments described below were conducted for a total treatment time of 120 minutes, as this duration was sufficient to resolve the relevant degradation kinetics and mechanistic trends.

Liquid phase products followed a characteristic evolution profile where the concentrations C_4-C_7 compounds increased during the first 40 minutes of the experiment and subsequently decreased as treatment progressed. In contrast, the concentrations of C_2 and C_3 compounds continually increased and did not exhibit significant degradation over the treatment duration. Concentrations of all PFOA byproducts remained low (< 0.8 mg/L for each shorter-chain compound) which is consistent with fluoride being the dominant transformation byproduct.

The rate of fluoride ion accumulation was highest within the first 60 minutes of treatment and decreased progressively thereafter (Fig. 2b). At 180 minutes, the fluoride ion concentration reached ~0.24 mM (corresponding

to ~65% fluoride yield) at 45 W and 0.29 mM (~80% fluoride yield) at 60 W for a liquid flowrate of 15 mL/min. To our knowledge, such high fluoride yields have not previously been reported for RF atmospheric-pressure plasma jet systems treating PFOA. In contrast, bubbling plasma reactors typically exhibit rapid initial defluorination followed by early kinetic saturation, with fluoride yields commonly plateauing near ~40-60% once the parent PFAS is degraded, and the remaining fluorine resides predominantly in stable, partially fluorinated byproducts that persist in the bulk liquid and are not further defluorinated [5, 13]. The continued increase in fluoride release observed here indicates sustained interfacial reactivity under APPJ conditions, with defluorination occurring predominantly from the parent PFAS rather than from secondary byproducts. This behavior is evident in Fig. 2 and confirmed further below, where the continued increase in fluoride release closely follows the degradation of the parent PFAS. Comparable fluoride yields have only been achieved in mesoporous plasma and microwave plasma reactors [33, 34].

Fig. 4b shows the distribution of measured fluorine among PFOA, the identified degradation byproducts, and free fluoride (expressed as the molar fraction of fluorine relative to the initial fluorine bound to PFOA) as a function of treatment time. Fluoride accumulation closely follows the degradation of parent PFOA, with >70% of the initial fluorine converted to F^-, while all identified short-chain PFAAs collectively account for <15% of the fluorine mass balance. While the rapid decrease in PFOA (and subsequent decrease of PFHpA) coincides with the largest increase in free fluoride, this is partially attributed to the high fluorine stoichiometry of the C8 molecule (15 F atoms) compared to short-chain intermediates like TFA (3 F atoms). Furthermore, the consistently low concentrations of C_2-C_4 products may indicate a pseudo-steady state, where their rate of formation from longer chains is balanced by their subsequent defluorination. Although their weak interfacial presence likely reduces their susceptibility to plasma-assisted degradation compared to PFOA, their role as transient intermediates in the total defluorination pathway cannot be ruled out [13, 35]. As shown in Fig. 5, organically bound fluorine decreases steadily during treatment, driven primarily by degradation of PFOA and PFHpA. After 2 h, fluoride ions account for ~70% of the total fluorine and PFAAs for ~12%. The remaining ~17% of fluorine, which may include gaseous, adsorbed, or unidentified liquid-phase byproducts, was generated early in the treatment and persisted throughout, suggesting limited susceptibility to further transformation under the present conditions [36].

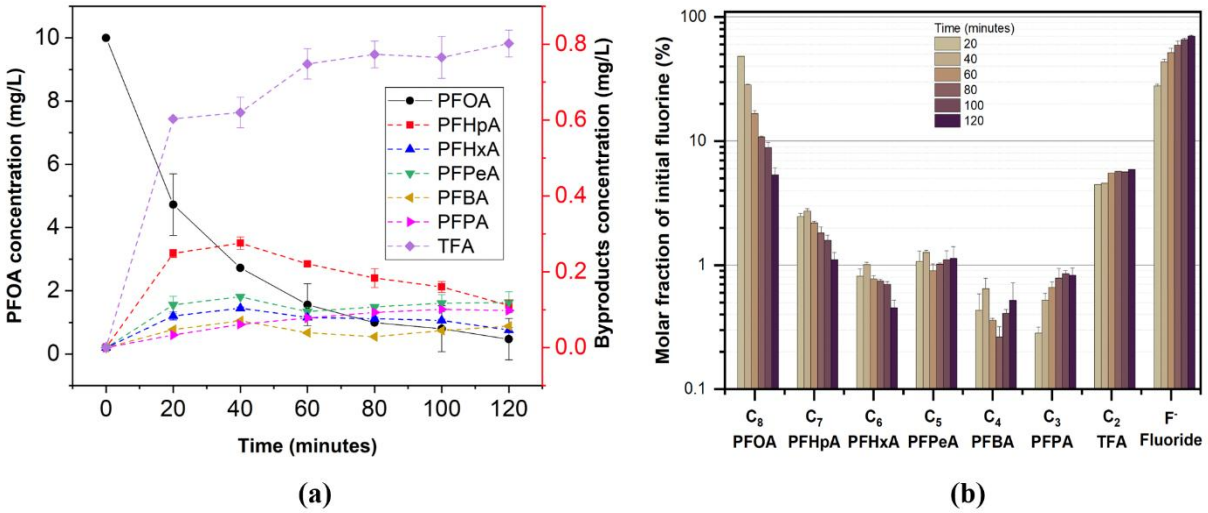


Fig. 4 Time-dependent (a) concentration profiles of PFOA and its byproducts and **(b)** molar fraction of initial fluorine (log scale) for the identified PFAAs at 60 W input power and 15 mL/min liquid flowrate for the first two hours of treatment time. The heights of the bars in (b) were estimated as $(\sum(C_i(t) \times f_i) / (C_0 \times f)) \times 100\%$, assuming an initial concentration of C_0 [mol/L] and no fluoride at t = 0 for a PFAAs molecule having the molecular formula $C_cF_fO_oH_h$. Here, i denotes the fluorine content bound within a particular byproduct where f_i is the number of fluorine atoms in that byproduct.

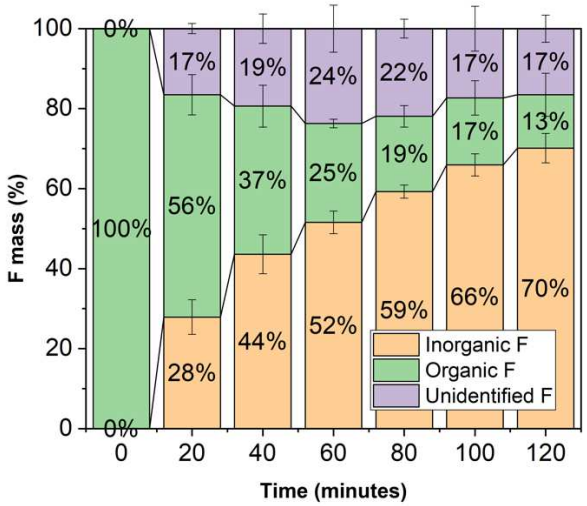


Fig. 5 Time-dependent mass fraction of initial fluorine at 60 W input power and 15 mL/min liquid flowrate for the first two hours treatment time. The heights of the bar for organic fluoride were estimated as $(\sum(C_i(t) \times f_i) / (C_0 \times f)) \times 100\%$, assuming an initial concentration of C_0 [mol/L] and no fluoride at t = 0 for a PFAAs molecule having the molecular formula $C_cF_fO_oH_h$. Here, i denotes the fluorine content bound within a particular byproduct where f_i is the number of fluorine atoms in that byproduct.

3.2 The effect of ·OH and e_{aq}^- scavengers on the degradation and defluorination of PFOA

Hydroxyl radicals have not been found to initiate the degradation of PFAS, but they have been extensively documented as playing a critical role in later phases of the reaction pathway, ultimately facilitating mineralization [37, 38]. In this study, phenol, a well-known OH scavenger ($k = 1.8 \times 10^{10}$ M^{-1} s^{-1} [39]), was introduced into the PFOA solution at varying concentrations (reported as PFOA: phenol molar ratios). The results revealed that its addition had no apparent effect on the degradation of PFOA (Fig. 6a) which is consistent with the very low rate constant for reaction between PFOA and OH ($\leq 1 \times 10^5$ M^{-1} s^{-1} [39]).

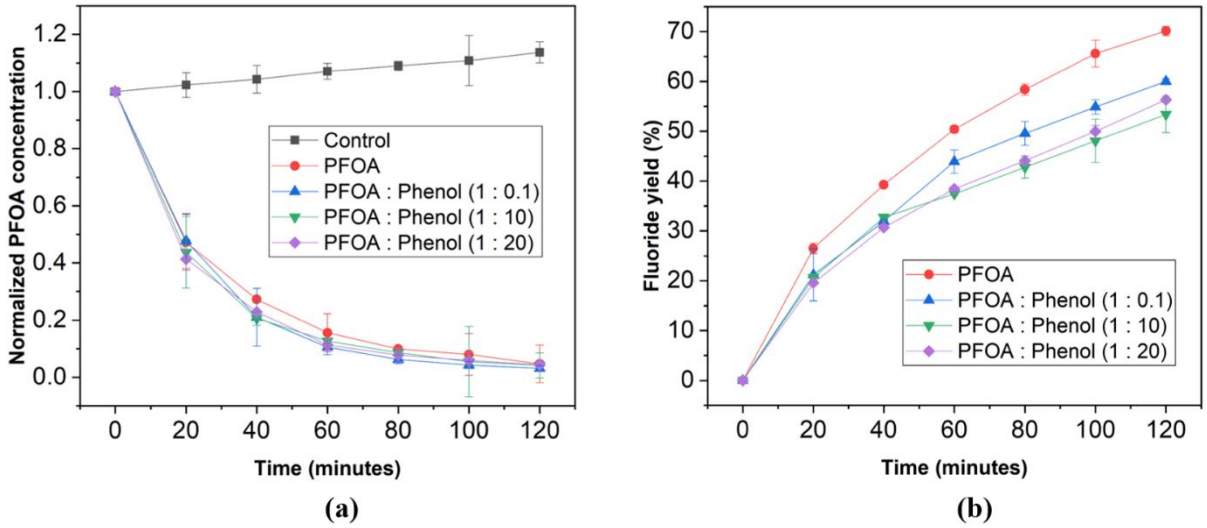


Fig. 6 Time-dependent (a) normalized PFOA concentration and (b) overall fluoride yield (%) of PFOA with and without the presence of varying molar ratios of phenol at 60 W input power and 15 mL/min liquid flowrate.

In contrast, the presence of phenol strongly affected the defluorination process (Fig. 6b). As the concentration of phenol increased, the rate of fluoride release gradually decreased from ~70% without the phenol to ~53% when phenol was present (1:10 case). Because phenol had no effect on PFOA degradation but significantly suppressed fluoride release, these results indicate that hydroxyl radicals are not responsible for initiating PFOA degradation but instead contribute to secondary oxidation and defluorination of partially fluorinated intermediates formed after the initial plasma-assisted cleavage [15, 29, 36]. This behavior is consistent with a reaction pathway in which initial C-F and C-C bond cleavage occurs at or very near the plasma-liquid interface. Owing to its amphiphilic nature, PFOA preferentially orients at the interface, with the hydrophilic carboxylate headgroup remaining solvated and the fluorinated tail extending toward the gas phase. This configuration places the fluorocarbon chain within the penetration depth of plasma-generated species, while rendering the primary interfacial degradation step insensitive to bulk-phase

scavengers such as phenol. In contrast, hydroxyl radicals diffusing away from the interface are effectively scavenged by phenol, selectively suppressing secondary oxidation pathways without influencing the initial degradation of PFOA.

The fluorine mass balance (Fig. 5) indicates that ~17% of the initial fluorine is not recovered as F^- or as the quantified PFAAs, consistent with formation of unidentified organofluorine (e.g., partially defluorinated intermediates and non-target fluorinated products) and/or minor volatile fluorine-containing species [29, 36]. Comparison of fluoride yields with and without phenol provides further insight into the fate of these intermediates. In the absence of phenol, the continued increase in fluoride yield beyond the rapid loss of parent PFOA indicates that a limited fraction of residual fluorine, initially retained in partially defluorinated intermediates, becomes accessible to secondary oxidation. This process contributes incrementally to total fluoride release but does not represent the dominant defluorination pathway [39–41]. However, when phenol is present, the scavenging of hydroxyl radicals suppresses this secondary oxidation pathway, leading to a ~17% reduction in total fluoride yield and a significant decrease in the cumulative fluorine yield within identified short-chain PFAAs from ~12% to ~3% (Fig. 7). This implies that in the presence of phenol, the unidentified fluorine fraction nearly doubles to approximately 44% (100% - 53% F^- - 3% PFAA-F), representing intermediates that are trapped in the bulk solution and cannot undergo further chain-shortening or defluorination.

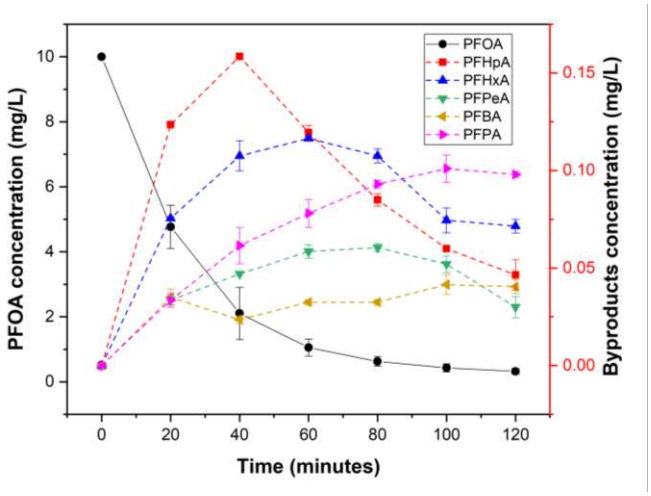


Fig. 7 Time-dependent concentration profiles of PFOA and its byproducts in the presence of phenol (PFOA: phenol = 1:10). 60 W input power and 15 mL/min liquid flowrate.

Plasma-generated chemically reductive species, such as solvated electrons (e^-_{aq}) and hydrogen atoms (H), have also been proposed to play a role in the primary dissociation reactions of PFOA [5, 42, 43]. To evaluate their contribution, silver nitrate ($AgNO_3$), a well-known scavenger for solvated electrons and, to a lesser extent, for

hydrogen radicals [44, 45], was introduced at varying concentrations. Its presence exhibited a minimal effect on both the degradation and defluorination profiles of PFOA (Fig. 8).

This result should not be interpreted as evidence against electron-driven degradation pathways. Solvated electrons and hot electrons generated at the plasma-liquid boundary exist within an ultrathin interfacial region on the order of a few *nm*, whereas ionic scavengers such as Ag^+ are largely excluded from this region due to electrostatic barriers, sheath formation, and short electron penetration depths [45]. The minimal effect of $AgNO_3$ therefore may reflect restricted interfacial accessibility of bulk phase ionic scavengers rather than the lack of aqueous reductive pathways.

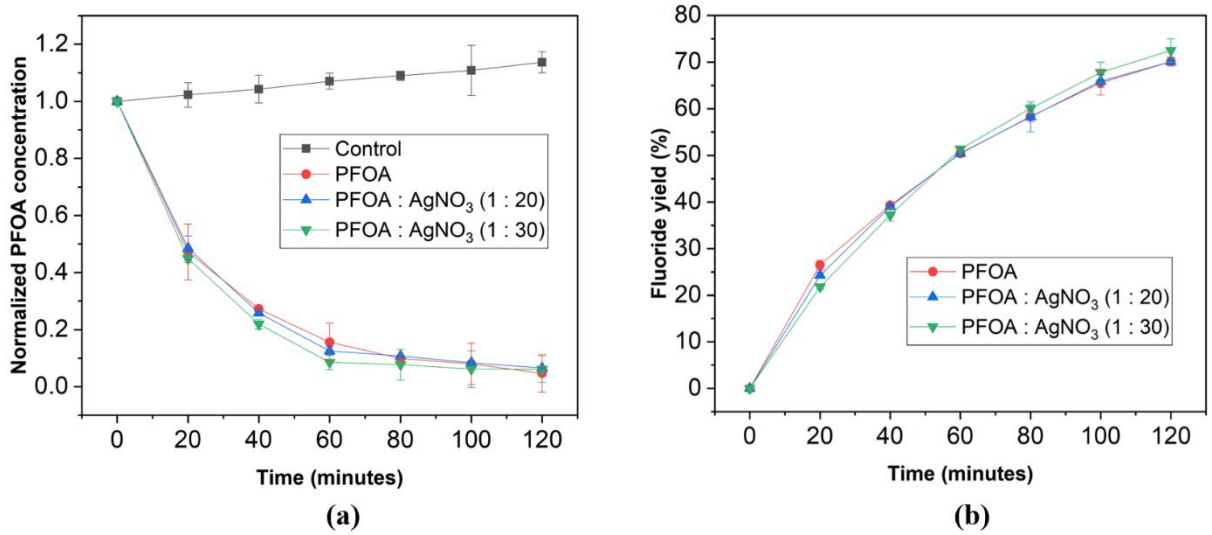


Fig. 8 Time-dependent (a) normalized PFOA concentration and (b) overall fluoride yield (%) of PFOA with and without the presence of varying molar ratios of $AgNO_3$ at 60 W input power and 15 mL/min liquid flowrate.

3.3 The effect of gas type on the degradation and defluorination of PFOA

To evaluate the influence of discharge gas composition on PFOA degradation and defluorination, argon was replaced with two admixtures (1% H_2 balanced with argon and 0.4% N_2 balanced with argon) and pure helium. The free jet length, measured from the nozzle exit without a substrate, was ~4 mm for argon, and decreased to ~3 mm with hydrogen and ~2 mm with both nitrogen and helium. Since the nozzle-to-substrate distance was fixed at 2 mm, and the presence of a substrate enhances plasma stability and coupling, plasma-liquid contact was maintained for all gas compositions.

Replacing argon with small hydrogen or nitrogen admixtures resulted in no appreciable change in PFOA removal, whereas helium significantly decreased both degradation and defluorination (Fig. 9). Defluorination followed the order Ar ≈ Ar + H_2 > Ar + N_2 >> He.

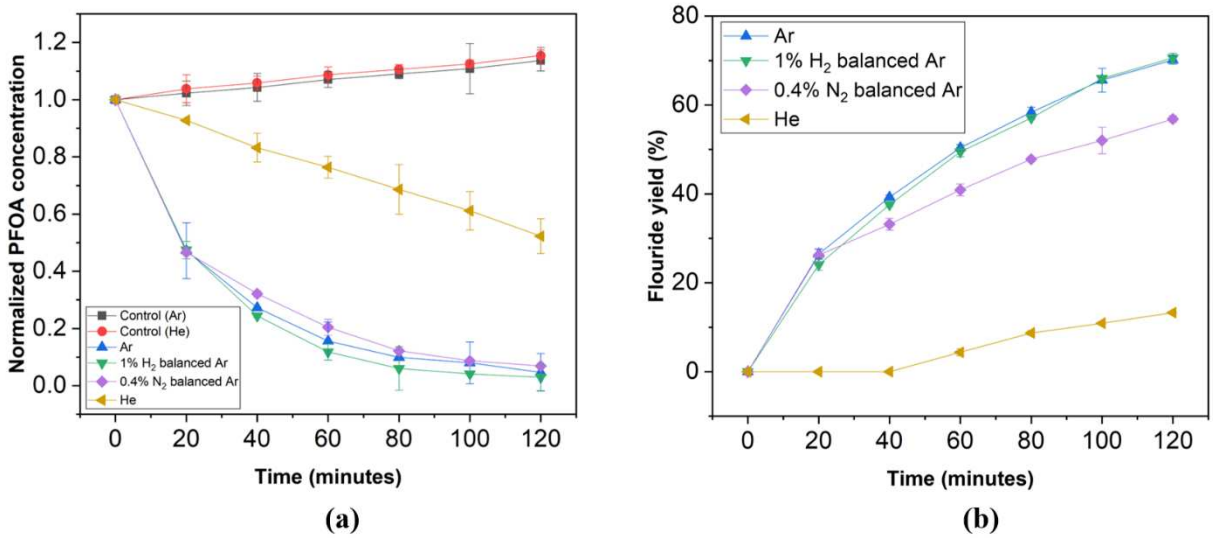


Fig. 9 Time-dependent (a) normalized PFOA concentration and (b) overall fluoride yield (%) of PFOA at 60 W input power and 15 mL/min liquid flowrate for 1% H_2 balanced Ar, 0.4% N_2 balanced Ar, and helium as processing gases. The gas flowrate was 0.8 SLM for all cases except for helium (2.3 SLM).

Argon plasmas are characterized by high electron density, strong localization of electric fields near the plasma-liquid interface, and intense emission of VUV radiation dominated by Ar_2*excimer emission near 125 nm (~9.9 eV) [46–48]. These conditions favor interfacial dissociation pathways involving both hot electrons and VUV photons, which possess sufficient energy to cleave C-F bonds (≈5.5 eV) and C-C bonds (≈3.9 eV) in surface-adsorbed PFOA molecules [21, 49–52]. The high efficiency of the argon discharge may also be attributed to the lower ionization potential of Ar (15.7 eV) relative to He (24.6 eV), allowing for a higher fraction of the input power to be channeled into electron-impact ionization and excitation rather than sustaining the plasma volume. Because PFOA is strongly surface-active, its fluorinated chain is preferentially exposed within the penetration depth of plasma-generated electrons and photons, making interfacial reactions highly efficient.

In contrast, the direct contribution of argon metastables and ions is substantially diminished under humid atmospheric-pressure conditions. Argon metastables are efficiently quenched by water vapor via Penning ionization and dissociative quenching which reduces their lifetimes from μs to tens of ns and suppresses Ar_2* formation [53].

Similarly, argon ions have mean free paths of only tens of nm at 1 atm and rapidly undergo charge-transfer and clustering reactions, resulting in thermalized species such as ArH^+ or H_2O^+ with kinetic energies < ~1 eV before reaching the liquid surface [54–56]. While such ions may contribute indirectly by initiating secondary radical chemistry near the interface, their direct role in C-F bond cleavage is expected to be limited.

The addition of small amounts of hydrogen (1% H_2 in Ar) did not enhance PFOA degradation or defluorination. While hydrogen admixtures (typically 0.5-5.0%) are often introduced to promote reductive chemistry through formation of atomic hydrogen or solvated electrons [57], the absence of an observable effect here suggests that the interfacial density of reactive species in pure Ar is already near a "saturation point" for the available surface-adsorbed PFOA. Any incremental increase in H-atom or solvated electron flux generated by hydrogen addition is likely negligible relative to the existing fluxes of electrons and VUV photons inherent to the argon discharge [58, 59]. In contrast, the addition of 0.4% nitrogen resulted in a modest but measurable decrease in defluorination efficiency. Nitrogen effectively quenches argon metastable states and Ar_2* excimers through collisional energy transfer, thereby suppressing VUV photon production [60]. In addition, nitrogen introduces new electron energy loss channels via vibrational and electronic excitation, which lowers the mean electron energy and suppresses high-energy electron-driven reactions such as dissociative electron attachment and direct bond scission [61]. Nitrogen-containing plasmas also favor NO_x formation, which can scavenge reactive oxygen species and further reduce secondary oxidation processes [62, 63].

Replacing argon with helium resulted in significant reduction in both degradation and defluorination. Although helium plasmas generate higher-energy photons (59-100 nm), the net VUV photon flux incident on the liquid surface under humid atmospheric-pressure conditions is substantially lower due to weaker excimer formation, enhanced collisional quenching, and reduced plasma-liquid coupling [19]. In addition, helium RF jets typically operate at lower electron densities (10^{17}-10^{18} m^{-3} vs. 10^{19}-10^{20} m^{-3} for argon) and exhibit broader, more diffuse discharge structures, which reduce electric field localization and the flux of electrons to the liquid surface [64, 65]. To compensate for these diffuse characteristics and maintain plasma-liquid contact, the helium flowrate was increased from 0.8 to 2.3 SLM. However, the adjustment likely introduced a gas-phase shielding effect; the resulting high-velocity inert gas layer increases convective losses of reactive species before they can reach the interface. Consequently, the combination of a lower primary species flux (electrons and photons) and increased shielding of

bulk-phase radicals suppresses the interfacial dissociation pathways necessary to break the PFOA monolayer, leading to the observed decrease in efficiency relative to argon.

Voltage-current waveforms (Fig. 10) provide further insight into the observed gas effects. Helium discharges exhibited lower peak currents (~6.4 mA) compared to argon (~10.8 mA) and lacked the high-frequency oscillations characteristic of more energetic argon plasmas. These features are consistent with lower electron densities, reduced sheath power deposition, and weaker electron acceleration toward the plasma-liquid interface in helium discharges [66]. In addition, the helium plasma plume was significantly broader (~675 ± 80 μm) than the argon plume (~340 ± 80 μm) [64], promoting radial diffusion losses and reducing localization of electric fields and reactive fluxes at the interface. In contrast, argon discharges produce a more constricted jet with stronger interfacial electric fields, higher electron fluxes, and enhanced generation of electrons and VUV photons, all of which favor efficient dissociation of surface-active PFOA. The higher axial gas velocity of the argon jet (~40 m s^{-1} compared to ~12 m s^{-1} for helium) further promotes interfacial renewal through liquid surface deformation, an effect shown previously to enhance plasma-liquid reaction rates [18]. Consistent with these discharge characteristics, the strong dependence of PFOA removal and fluoride release on applied RF power (Fig. 2) supports a mechanism in which initiation is governed by power-sensitive interfacial processes, most notably electron-driven and electron-coupled pathways, rather than by bulk aqueous-phase chemistry or mass transport limitations.

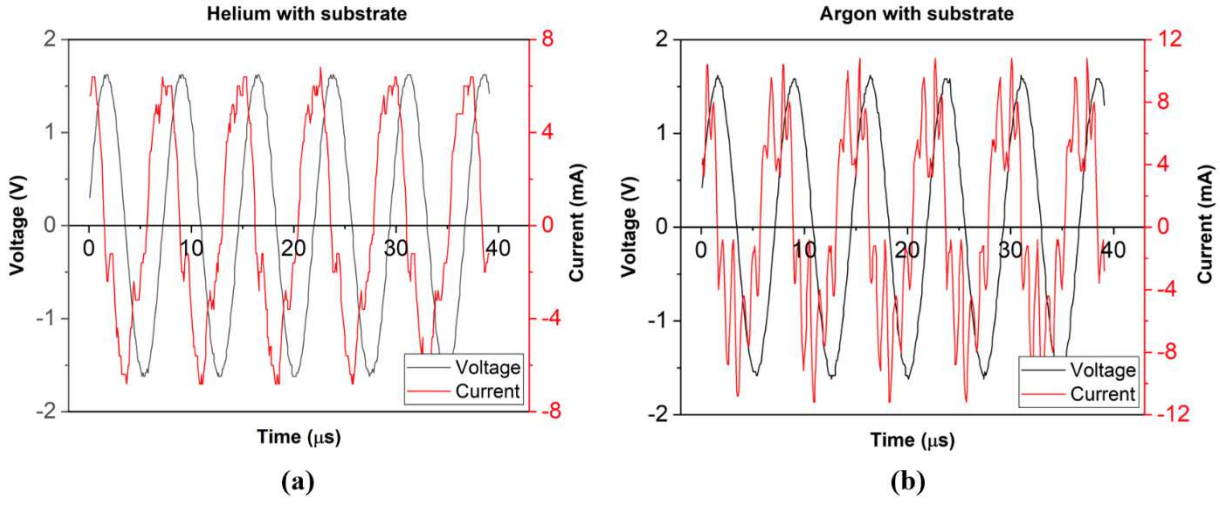


Fig. 10 Time-dependent voltage-current waveforms for two distinct conditions: (a) helium plasma with flow-through cuvette reactor containing PFOA and (b) argon plasma with flow-through cuvette reactor containing PFOA for 15 mL/min liquid flowrate. Gas flowrate was 2.3 SLM and 0.8 SLM for helium and argon respectively.

4. Conclusions

This study elucidates the mechanisms governing PFOA degradation and defluorination in RF atmospheric-pressure plasma jets by systematically correlating reactor operating conditions, scavenger effects, and gas composition to interfacial plasma-liquid processes. The parent PFOA was removed to below detection within two hours, while fluoride release continued and reached up to ~80% after three hours. Identified short-chain perfluoroalkyl acids (C_2-C_7) accounted for ~12% of the initial mass. Increasing RF power enhanced both, PFOA removal and defluorination, whereas varying liquid recirculation rate had minimal impact, indicating that performance is controlled by interfacial delivery of plasma-generated species rather than bulk hydrodynamic transport.

Consistent with this interpretation, the addition of an OH radical scavenger had no effect on the PFOA degradation but decreased fluoride yield by ~17% and reduced the cumulative yield of short-chain PFAAs from ~12% to ~3%. This decoupling of parent removal from defluorination indicates that hydroxyl radicals do not participate in the initiation of PFOA degradation, but instead promote secondary oxidation, chain-shortening, and incremental C-F bond cleavage of partially defluorinated intermediates formed following interfacial plasma-driven dissociation. In contrast, the addition of $AgNO_3$ produced minimal changes in either degradation or defluorination kinetics, consistent with the limited accessibility of bulk-phase ionic scavengers to the *nm*-scale plasma-liquid interfacial reaction zone where electron- and photon-driven processes dominate. Gas composition further affected degradation and defluorination by controlling interfacial electron and photon fluxes through changes in electron density, discharge localization and VUV photon production. Among the gases investigated, argon provided the most favorable conditions due to its higher electron density and strong Ar_2* excimer emission, leading to superior performance relative to helium and gas-admixture conditions.

These results suggest that PFOA degradation and defluorination in RF plasma jets are controlled primarily by interfacial electron- and photon-mediated pathways, with aqueous-phase radical chemistry contributing at later stages. Future work combining experiments with self-consistent plasma-fluid and plasma-liquid interface modeling will be critical to quantitatively verify these interpretations and to resolve the relative contributions of electron- and photon-driven pathways. More broadly, these mechanistic conclusions should not be generalized across all plasma reactors, since different plasma sources generate different reactive species distributions and exhibit different modes

of coupling to the plasma-liquid interface. Accordingly, the dominant PFAS degradation mechanism may vary considerably from one plasma platform to another, depending on the species produced and the way in which they are delivered to the interface.

Although RF atmospheric-pressure plasma jets are not suited for large-volume PFAS treatment, they provide a highly controlled platform for isolating elementary plasma-liquid interfacial processes. Insights gained from these systems are therefore critical for informing the design and optimization of scalable plasma-based PFAS remediation technologies.

Statements and Declarations

Competing Interest

The authors declare the following financial interests/personal relationships, which may be considered as potential competing interests: Selma Mededovic reports financial support was provided by U.S. Department of Energy and the National Science Foundation.

Data Availability

The datasets generated during and/or analyzed during the current study are available from the corresponding author on reasonable request.

Acknowledgements

This work is supported by the U.S. Department of Energy, Office of Science, Office of Fusion Energy Sciences, General Plasma Science (Award Number DE-SC-0020232), and the National Science Foundation ECO-CBET (Award Number 2318494) and ECLIPSE (Award Number 2308858) Programs.

Author Contributions

M.R. conceptualized and conducted the study, analyzed the experimental data, and contributed to manuscript preparation and revisions. T.H. offered expertise in data analysis and contributed to manuscript review. S.M.T. supervised the research, provided guidance on experimental design and data analysis, contributed to manuscript writing and revisions, and served as the corresponding author. All authors have reviewed and approved the final draft of the manuscript.

References

1. Cao X, Wang C, Lu Y, et al (2019) Occurrence, sources and health risk of polyfluoroalkyl substances (PFASs) in soil, water and sediment from a drinking water source area. Ecotoxicol Environ Saf 174:208–217. https://doi.org/10.1016/j.ecoenv.2019.02.058
2. Stratton GR, Dai F, Bellona CL, et al (2017) Plasma-Based Water Treatment: Efficient Transformation of Perfluoroalkyl Substances in Prepared Solutions and Contaminated Groundwater. Environ Sci Technol 51:1643–1648. https://doi.org/10.1021/acs.est.6b04215
3. Watkins DJ, Josson J, Elston B, et al (2013) Exposure to perfluoroalkyl acids and markers of kidney function among children and adolescents living near a chemical plant. Environ Health Perspect 121:625–630. https://doi.org/10.1289/ehp.1205838
4. U.S. Environmental Protection Agency (2024) PFAS National Primary Drinking Water Regulation. Federal Register 89(82):32532–32757. https://www.federalregister.gov/documents/2024/04/26/2024-07773/pfas-national-primary-drinking-water-regulation. Accessed 20 Nov 2025
5. Singh RK, Fernando S, Baygi SF, et al (2019) Breakdown Products from Perfluorinated Alkyl Substances (PFAS) Degradation in a Plasma-Based Water Treatment Process. Environ Sci Technol 53:2731–2738. https://doi.org/10.1021/acs.est.8b07031
6. Singh RK, Multari N, Nau-Hix C, et al (2019) Rapid Removal of Poly- and Perfluorinated Compounds from Investigation-Derived Waste (IDW) in a Pilot-Scale Plasma Reactor. Environ Sci Technol. https://doi.org/10.1021/acs.est.9b02964
7. Nau-Hix C, Multari N, Singh RK, et al (2021) Field Demonstration of a Pilot-Scale Plasma Reactor for the Rapid Removal of Poly- and Perfluoroalkyl Substances in Groundwater. ACS ES and T Water 1:680–687. https://doi.org/10.1021/acsestwater.0c00170
8. Tang H, Xiang Q, Lei M, et al (2012) Efficient degradation of perfluorooctanoic acid by UV-Fenton process. Chemical Engineering Journal 184:156–162. https://doi.org/10.1016/j.cej.2012.01.020
9. Giri RR, Ozaki H, Okada T, et al (2012) Factors influencing UV photodecomposition of perfluorooctanoic acid in water. Chemical Engineering Journal 180:197–203. https://doi.org/10.1016/j.cej.2011.11.049
10. Zhuo Q, Deng S, Yang B, et al (2011) Efficient electrochemical oxidation of perfluorooctanoate using a Ti/SnO2-Sb-Bi anode. Environ Sci Technol 45:2973–2979. https://doi.org/10.1021/es1024542
11. Kim TH, Yu S, Choi Y, et al (2018) Profiling the decomposition products of perfluorooctane sulfonate (PFOS) irradiated using an electron beam. Science of the Total Environment 631–632:1295–1303. https://doi.org/10.1016/j.scitotenv.2018.03.055
12. Zhang Z, Chen JJ, Lyu XJ, et al (2014) Complete mineralization of perfluorooctanoic acid (PFOA) by γ-irradiation in aqueous solution. Sci Rep 4:7418. https://doi.org/10.1038/srep07418
13. Isowamwen O, Li R, Holsen T, Thagard SM (2023) Plasma-assisted degradation of a short-chain perfluoroalkyl substance (PFAS): Perfluorobutane sulfonate (PFBS). J Hazard Mater 456:131691. https://doi.org/10.1016/j.jhazmat.2023.131691

14. Lewis AJ, Joyce T, Hadaya M, et al (2020) Rapid degradation of PFAS in aqueous solutions by reverse vortex flow gliding arc plasma. Environ Sci (Camb) 6:1044–1057. https://doi.org/10.1039/c9ew01050e
15. Topolovec B, Jovanovic O, Puac N, et al (2024) Plasma water treatment for PFAS: Study of degradation of perfluorinated substances and their byproducts by using cold atmospheric pressure plasma jet. J Environ Chem Eng 12:112979. https://doi.org/10.1016/j.jece.2024.112979
16. Nayak G, Oinuma G, Yue Y, et al (2021) Plasma-droplet interaction study to assess transport limitations and the role of ·OH, O·,H·,O2(a1Δg),O3, He(23S) and Ar(1s5) in formate decomposition. Plasma Sources Sci Technol 30:115003. https://doi.org/10.1088/1361-6595/ac2676
17. Kondeti VSSK, Bruggeman PJ (2021) The interaction of an atmospheric pressure plasma jet with liquid water: Dimple dynamics and its impact on crystal violet decomposition. J Phys D Appl Phys 54:045204. https://doi.org/10.1088/1361-6463/abbeb5
18. Taghvaei H, Kondeti VSSK, Bruggeman PJ (2019) Decomposition of Crystal Violet by an Atmospheric Pressure RF Plasma Jet: The Role of Radicals, Ozone, Near-Interfacial Reactions and Convective Transport. Plasma Chemistry and Plasma Processing 39:729–749. https://doi.org/10.1007/s11090-019-09965-w
19. Nayak G, Wang J, Li R, et al (2023) Non-OH-driven liquid-phase chemistry in water microdroplets. Plasma Processes and Polymers 20:2200222. https://doi.org/10.1002/ppap.202200222
20. Levenspiel O (1999) Chemical reaction engineering, 3rd ed. John Wiley & Sons, New York
21. Bentel MJ, Yu Y, Xu L, et al (2019) Defluorination of Per- and Polyfluoroalkyl Substances (PFASs) with Hydrated Electrons: Structural Dependence and Implications to PFAS Remediation and Management. Environ Sci Technol 53:3718–3728. https://doi.org/10.1021/acs.est.8b06648
22. Lukes P, Appleton AT, Locke BR (2004) Hydrogen Peroxide and Ozone Formation in Hybrid Gas-Liquid Electrical Discharge Reactors. IEEE Trans Ind Appl 40:60–67. https://doi.org/10.1109/TIA.2003.821799
23. Alfianto E, Ikuse K, Donkó Z, Hamaguchi S (2025) Numerical simulation of chemical reactions in phosphate-buffered saline (PBS) exposed to helium pulsed plasmas at atmospheric pressure. Jpn J Appl Phys 64:046002. https://doi.org/10.35848/1347-4065/adc6d5
24. Moradi H, Kim DS, Kim SH, et al (2022) Experimental and numerical study on diazinon removal using plasma bubble column reactor: Modeling, kinetics, mechanisms, and degradation products. J Environ Chem Eng 10:108291. https://doi.org/10.1016/j.jece.2022.108291
25. Kruszelnicki J, Lietz AM, Kushner MJ (2019) Atmospheric pressure plasma activation of water droplets. J Phys D Appl Phys 52:355207. https://doi.org/10.1088/1361-6463/ab25dc
26. Vasilev M, Suiter J, Bohl D, Thagard SM (2023) Caffeine degradation in a plasma-liquid reactor with the lateral liquid flow: Elucidating the effects of mass transport on contaminant removal. Chemical Engineering Journal 473:144833. https://doi.org/10.1016/j.cej.2023.144833
27. Nau-Hix C, Holsen TM, Mededovic Thagard S (2022) Optimization of a gas–liquid plasma reactor for water treatment applications: Design guidelines and electrical circuit considerations. Plasma Processes and Polymers 19:2200036. https://doi.org/10.1002/ppap.202200036

28. Haghshenasfard M, Schönekerl S, Scale G, et al (2025) Experimental and CFD analysis of two-phase flow in a ceramic porous media under plasma-assisted wastewater treatment conditions. Chemical Engineering Research and Design 223:160–176. https://doi.org/10.1016/j.cherd.2025.09.030
29. Tomei G, Saleem M, Scalvini F, et al (2025) Fluorine Substitution and CO2 Production in the Treatment of Perfluorooctanoic Acid in a Radial Plasma Discharge Reactor. Plasma Chemistry and Plasma Processing 2025 46:1 46:10-. https://doi.org/10.1007/s11090-025-10633-5
30. Tomei G, Piva E, Saleem M, et al (2025) Optimization and Testing of an SPE-LC/q-TOF Analytical Method for the Detection of PFAS Degradation Products in Water Treatment Processes. Environ Sci Technol 59:22251–22261. https://doi.org/10.1021/acs.est.5c01886
31. Biondo O, Tomei G, Saleem M, et al (2023) Products, reactive species and mechanisms of PFOA degradation in a self-pulsing discharge (SPD) plasma reactor. Chemosphere 341:139972. https://doi.org/10.1016/j.chemosphere.2023.139972
32. Song C, Zhao Y, Liu Z, et al (2025) Plasma-Generated Free Electrons Induced Perfluorooctanoic Acid Efficient Degradation at the Gas–Liquid Interface. Environ Sci Technol 59:9332–9343. https://doi.org/10.1021/acs.est.5c02062
33. Guo J, Zhang Y, Sun Q, et al (2022) Theoretical and experimental insights into electron-induced efficient defluorination of perfluorooctanoic acid and perfluorooctane sulfonate by mesoporous plasma. Chemical Engineering Journal 430:132922. https://doi.org/10.1016/j.cej.2021.132922
34. Sun S, Sun B, Wang Q, et al (2023) Efficient defluorination of PFOA by microwave discharge plasma in liquid: Influence of actual water environment factors. Journal of Water Process Engineering 55:104091. https://doi.org/10.1016/j.jwpe.2023.104091
35. Alam D, Lee S, Hong J, et al (2023) Experimental investigations of Per- and Poly-fluoroalkyl substances (PFAS) degradation by non-thermal plasma in aqueous solutions. J Environ Chem Eng 11:111588. https://doi.org/10.1016/j.jece.2023.111588
36. Aranzales D, Isowamwen O, Fernando S, et al (2025) Perfluorobutanesulfonate (PFBS) Treatment by Electrical Discharge Plasma: Reaction Mechanisms and Degradation Pathways. 10:37535. https://doi.org/10.1021/acsomega.5c03568
37. Kundu S, Radian A (2022) Surface confinement of per-fluoroalkyl substances on an iron-decorated clay-cyclodextrin composite enables rapid oxidation by hydroxyl radicals. Chemical Engineering Journal 431:134187. https://doi.org/10.1016/j.cej.2021.134187
38. Cheng J, Fan Y, Pei X, et al (2022) Mechanism and Reactive Species in a Fountain-Strip DBD Plasma for Degrading Perfluorooctanoic Acid (PFOA). Water (Switzerland) 14:3384. https://doi.org/10.3390/w14213384
39. Buxton G V., Greenstock CL, Helman WP, Ross AB (1988) Critical Review of rate constants for reactions of hydrated electrons, hydrogen atoms and hydroxyl radicals (·OH/·O− in Aqueous Solution. J Phys Chem Ref Data 17:513–886. https://doi.org/10.1063/1.555805

40. Gar Alalm M, Boffito DC (2022) Mechanisms and pathways of PFAS degradation by advanced oxidation and reduction processes: A critical review. Chemical Engineering Journal 450:138352. https://doi.org/10.1016/j.cej.2022.138352
41. Yang Y, Zheng Z, Yang M, et al (2020) In-situ fabrication of a spherical-shaped Zn-Al hydrotalcite with BiOCl and study on its enhanced photocatalytic mechanism for perfluorooctanoic acid removal performed with a response surface methodology. J Hazard Mater 399:123070. https://doi.org/10.1016/j.jhazmat.2020.123070
42. Takeuchi N, Kitagawa Y, Kosugi A, et al (2013) Plasma–liquid interfacial reaction in decomposition of perfluoro surfactants. J Phys D Appl Phys 47:045203. https://doi.org/10.1088/0022-3727/47/4/045203
43. Matsuya Y, Takeuchi N, Yasuoka K (2014) Relationship between reaction rate of perfluorocarboxylic acid decomposition at a plasma-liquid interface and adsorbed amount. Electrical Engineering in Japan (English translation of Denki Gakkai Ronbunshi) 188:1–8. https://doi.org/10.1002/eej.22526
44. Kondeti VSSK, Gangal U, Yatom S, Bruggeman PJ (2017) Ag+ reduction and silver nanoparticle synthesis at the plasma–liquid interface by an RF driven atmospheric pressure plasma jet: Mechanisms and the effect of surfactant. Journal of Vacuum Science & Technology A: Vacuum, Surfaces, and Films 35:061302. https://doi.org/10.1116/1.4995374
45. Rumbach P, Bartels DM, Sankaran RM, Go DB (2015) The solvation of electrons by an atmospheric-pressure plasma. Nat Commun 6:7248. https://doi.org/10.1038/ncomms8248
46. Golda J, Biskup B, Layes V, et al (2020) Vacuum ultraviolet spectroscopy of cold atmospheric pressure plasma jets. Plasma Processes and Polymers 17:1900216. https://doi.org/10.1002/ppap.201900216
47. El-Habachi A, Schoenbach KH (1998) Emission of excimer radiation from direct current, high-pressure hollow cathode discharges. Appl Phys Lett 72:22–24. https://doi.org/10.1063/1.120634
48. Kozhevnikov VV, Panchenko AN, Tarasenko VF (2022) UV and VUV radiation of rare gases and nitrogen in diffuse discharges, formed in an inhomogeneous electric field. 554–559. https://doi.org/10.56761/efre2022.s5-p-020803
49. Hildenbrand DL (1975) Dissociation Energy and Ionization potential of the molecule CF. Chem Phys Lett 32:523–526. https://doi.org/10.1016/0009-2614(75)85231-6
50. Blanksby SJ, Ellison GB (2003) Bond Dissociation Energies of Organic Molecules. Acc Chem Res 36:255–263. https://doi.org/10.1021/ar020230d
51. Jing C, Zhang P-Y, Liu J (2007) Photodegradation of perfluorooctanoic acid by 185 nm vacuum ultraviolet light. Journal of Environmental Sciences 19:387–390. https://doi.org/10.1016/S1001-0742(07)60064-3
52. Vanraes P, Bogaerts A (2021) The essential role of the plasma sheath in plasma-liquid interaction and its applications—A perspective. J Appl Phys 129:220901. https://doi.org/10.1063/5.0044905
53. Heneral AA, Avtaeva S V. (2020) Atmospheric pressure plasma jets generated by the DBD in argon-air, helium-air, and helium-water vapour mixtures. J Phys D Appl Phys 53:195201. https://doi.org/10.1088/1361-6463/ab7354

54. Bruggeman PJ, Kushner MJ, Locke BR, et al (2016) Plasma-liquid interactions: A review and roadmap. Plasma Sources Sci Technol 25:053002. https://doi.org/10.1088/0963-0252/25/5/053002
55. Phelps A V (1992) Collisions of H+, H2+, H3+, ArH+, H-, H, and H2 with Ar and of Ar+ and ArH+ with H2 for Energies from 0.1 eV to 10 keV. J Phys Chem Ref Data 21:883–897. https://doi.org/10.1063/1.555917
56. Albritton DL, Albrilton DL (1979) Ion-neutral reaction-rate constants measured in Flow reactors through 1977. At Data Nucl Data Tables 22:1–101. https://doi.org/10.1016/0092-640x(78)90027-x
57. Ellis WC, Lewis CR, Openshaw AP, Farnsworth PB (2016) The Effects of Added Hydrogen on Noble Gas Discharges Used as Ambient Desorption/Ionization Sources for Mass Spectrometry. J Am Soc Mass Spectrom 27:1539–1549. https://doi.org/10.1007/s13361-016-1432-y
58. Bogaerts A (2002) Hydrogen addition to an argon glow discharge: a numerical simulation. J Anal At Spectrom 17:768–779. https://doi.org/10.1039/b200025c
59. Bogaerts A, Gijbels R (2000) Effects of adding hydrogen to an argon glow discharge: overview of relevant processes and some qualitative explanations. J Anal At Spectrom 15:441–449. https://doi.org/10.1039/a909779a
60. Stefanović I, Kuschel T, Schröter S, Böke M (2014) Argon metastable dynamics and lifetimes in a direct current microdischarge. J Appl Phys 116:113302. https://doi.org/10.1063/1.4895714
61. Colonna G, Laporta V, Celiberto R, et al (2015) Non-equilibrium vibrational and electron energy distributions functions in atmospheric nitrogen ns pulsed discharges and μs post-discharges: the role of electron molecule vibrational excitation scaling-laws. Plasma Sources Sci Technol 24:035004. https://doi.org/10.1088/0963-0252/24/3/035004
62. Zhu D, Sun Z, Zhang H, et al (2022) Reactive Nitrogen Species Generated by Gas–Liquid Dielectric Barrier Discharge for Efficient Degradation of Perfluorooctanoic Acid from Water. Environ Sci Technol 56:349–360. https://doi.org/10.1021/acs.est.1c06342
63. Yuan Y, Feng L, Xie N, et al (2020) Rapid photochemical decomposition of perfluorooctanoic acid mediated by a comprehensive effect of nitrogen dioxide radicals and Fe3+/Fe2+ redox cycle. J Hazard Mater 388:121730. https://doi.org/10.1016/j.jhazmat.2019.121730
64. Brahme A, Chang Z, Zhao N, et al (2018) Penetration of Ar and He RF-driven plasma jets into micrometer-sized capillary tubes. J Phys D Appl Phys 51:414002. https://doi.org/10.1088/1361-6463/aad883
65. Tian P, Kushner MJ (2015) Controlling VUV photon fluxes in low-pressure inductively coupled plasmas. Plasma Sources Sci Technol 24:034017. https://doi.org/10.1088/0963-0252/24/3/034017
66. Shao XJ, Jiang N, Zhang GJ, Cao ZX (2012) Comparative study on the atmospheric pressure plasma jets of helium and argon. Appl Phys Lett 101:253509. https://doi.org/10.1063/1.4772639